Internal Electrostatic Control of the Primary Charge Separation and Recombination in Reaction Centers from Rhodobacter sphaeroides Revealed by Femtosecond Transient Absorption

ARTICLE *in* THE JOURNAL OF PHYSICAL CHEMISTRY B · JULY 2009

Impact Factor: 3.3 · DOI: 10.1021/jp811234q · Source: PubMed

5 AUTHORS, INCLUDING:

Krzysztof Gibasiewicz
Adam Mickiewicz University
26 PUBLICATIONS **391** CITATIONS
SEE PROFILE

Marcin Ziolek
Adam Mickiewicz University
53 PUBLICATIONS **823** CITATIONS
SEE PROFILE

Andrzej Dobek
Adam Mickiewicz University
56 PUBLICATIONS **444** CITATIONS
SEE PROFILE

Internal Electrostatic Control of the Primary Charge Separation and Recombination in Reaction Centers from *Rhodobacter sphaeroides* Revealed by Femtosecond Transient Absorption

K. Gibasiewicz,* M. Pajzderska, M. Ziółek, J. Karolczak, and A. Dobek

Department of Physics, Adam Mickiewicz University, ul. Umultowska 85, 61-614 Poznań, Poland

Received: December 19, 2008; Revised Manuscript Received: June 4, 2009

We report the observation of two conformational states of closed RCs from *Rhodobacter sphaeroides* characterized by different $P^+H_A^- \rightarrow PH_A$ charge recombination lifetimes, one of which is of subnanosecond value (700 ± 200 ps). These states are also characterized by different primary charge separation lifetimes. It is proposed that the distinct conformations are related to two protonation states either of reduced secondary electron acceptor, Q_A^-, or of a titratable amino acid residue localized near Q_A. The reaction centers in the protonated state are characterized by faster charge separation and slower charge recombination when compared to those in the unprotonated state. Both effects are explained in terms of the model assuming modulation of the free energy level of the state $P^+H_A^-$ by the charges on or near Q_A and decay of the $P^+H_A^-$ state via the thermally activated $P^+B_A^-$ state.

Introduction

Primary charge separation and primary charge recombination are two opposite reactions taking place in the photosynthetic reaction center (RC) and can be described by the following reaction scheme

$$P^{(*)}B_AH_A \leftrightarrow P^+B_A^-H_A \leftrightarrow P^+B_AH_A^- \qquad (1)$$

where P, a dimer of bacteriochlorophylls, is the primary electron donor, B_A, a monomeric bacteriochlorophyll, is an intermediate electron carrier, and H_A, a bacteriopheophytin, is the primary electron acceptor in RCs of purple bacteria.[1] The primary charge separation occurs mostly from the excited state of the primary donor, P*, and takes a few picoseconds (3−5 ps), whereas the charge recombination occurs predominantly to the ground state of P and is about 3 orders of magnitudes slower. The literature values of the rate of charge recombination measured by transient absorption are $(10-30\ \text{ns})^{-1}$ [2−7] and have been shown to be modulated by external magnetic field (see ref 8 for review).

A strong electrical field related to the appearance of the primary radical pair, $P^+H_A^-$, induces a dielectric response from the protein environment. This response (relaxation) stabilizes or shifts down the energy level of $P^+H_A^-$ and the process of this stabilization occurs on picosecond to nanosecond time scales.[7] The intermediate state, $P^+B_A^-$, is normally very weakly and only transiently populated, since its formation (3.5 ps) is slower than its decay (0.5 ps).[1] However, even when the primary charge separation is completed, a small fraction of the RCs is expected to be in the $P^+B_A^-$ state due to a thermal equilibrium with the state $P^+H_A^-$.

In a recent paper it was shown that the charge recombination is not a monophasic exponential process but can be modeled by three exponential components of <1, 3−4, and 9−12 ns.[9] This complex kinetics was explained by the model assuming that the recombination occurs predominantly from the $P^+B_A^-$ state being in equilibrium with $P^+H_A^-$ and separated from the latter state by three different free energy gaps (up to 170 meV deep) related to the respective conformational states of RCs. Due to a relatively low temporal resolution of the setup (∼1 ns), it was not possible to determine precisely either the exact lifetime or the exact relative amplitude of the fastest component. However, it was possible to find that the contributions of the fastest and slowest phases were strongly modulated by charges in the Q_A site. The highest contribution of the fastest phase was observed in the Q_A-reduced RCs and the lowest one in the Q_A-removed RCs. Addition of *o*-phenanthroline, a herbicide involved in protonation of titratable groups at the Q_A site,[10,11] decreased the relative contribution of the fastest phase.

In this paper, we will provide a more precise determination of the lifetime and relative contribution of the subnanosecond component of charge recombination. At the same time, we explore whether the internal electrostatic control provided by the charges at the Q_A site also influences the primary charge separation. Finally, we show that the previous model, derived from the kinetic data obtained for two wavelengths in the infrared,[9] can be successfully extended in order to account for many spectrotemporal features observed on the subnanosecond time scale in a wide spectral range from 330 to 700 nm.

Materials and Methods

RCs isolated from a His-tagged version of *Rb. sphaeroides* strain 2:4:1 were prepared according to the procedure described in ref 12. To remove the quinone from the Q_A site, we applied the procedure described in refs 13 and 14. Reduction of Q_A was realized by permanent continuous illumination of the sample during the transient absorption experiment, with a halogen lamp, after addition of 10 mM sodium ascorbate. Sodium ascorbate rereduced P^+ to P after formation of $P^+Q_A^-$ as a result of continuous illumination. The intensity of this illumination was set on a level which ensured elimination of the features characteristic of open RCs from the transient spectra. The effect of *o*-phenanthroline was studied after addition of 100 μL of

* To whom correspondence should be addressed. Tel.: +48 61 8295265. E-mail: krzyszgi@amu.edu.pl.

10.1021/jp811234q CCC: $40.75
Published on Web 07/15/2009

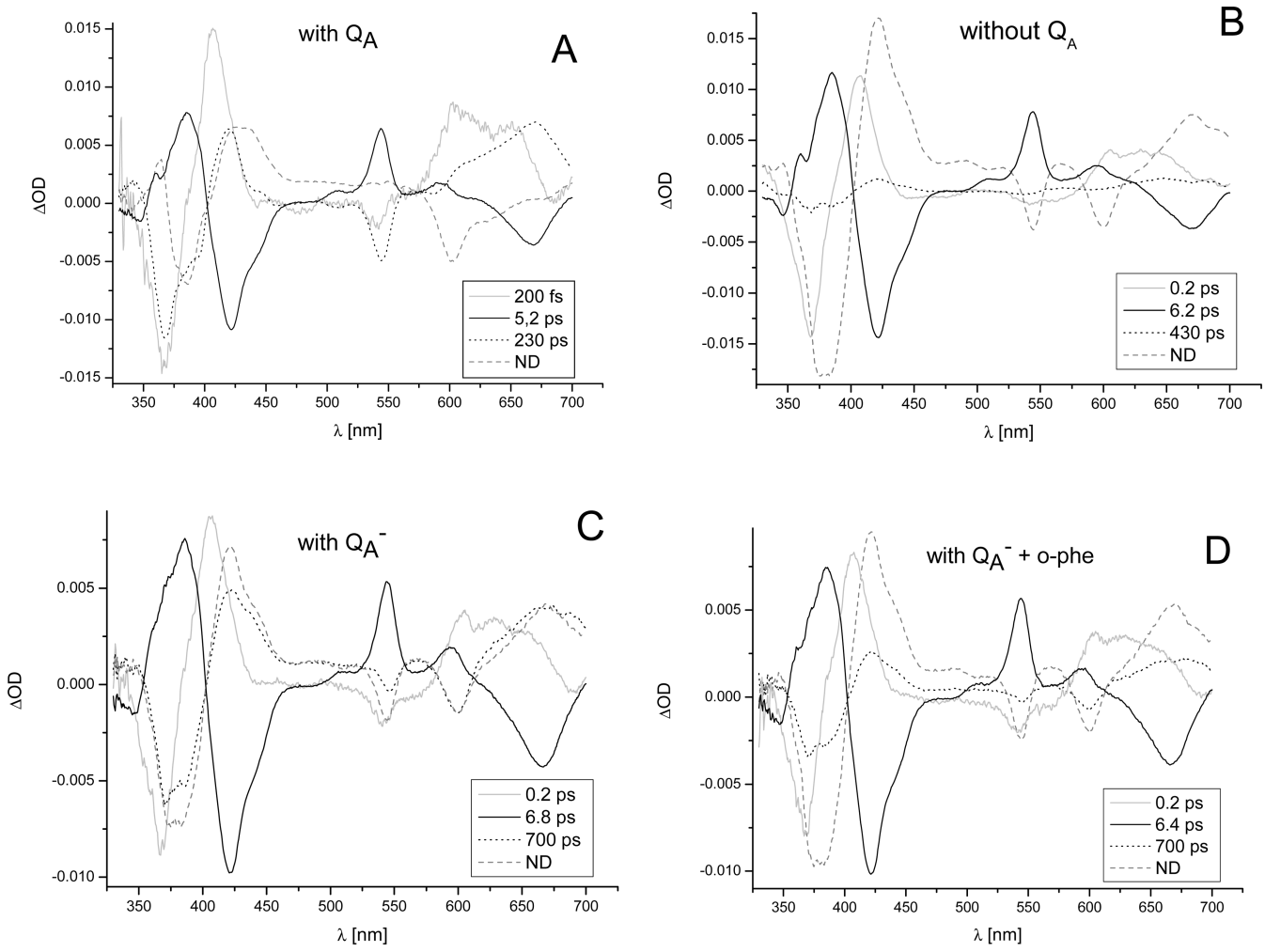

Figure 1. Decay-associated spectra found from the global analysis of the transient absorption spectra for *Rb. sphaeroides* RCs in the open state (A), in the closed state by removing Q_A (B), in the closed state by reducing Q_A (C), and in closed state by reducing Q_A and with addition of 10 mM *o*-phenanthroline (D). The lifetimes of the fastest, 200 fs, phases and of the charge recombination, 700 ps, phases were fixed in order to directly compare the shapes and amplitudes of DAS for different samples. Free fits gave similar lifetimes and only insignificantly lower chi-squared values.

stock solution of this herbicide yielding its final concentration of 10 mM. The experiments on open RCs, then on the Q_A-reduced RCs, first without and then in the presence of *o*-phenanthroline, were performed each time sequentially on the same sample and without any changes in the alignment of the setup.

For the transient absorption measurements, the stock solution containing RCs of $OD_{800\ nm} \approx 15\ cm^{-1}$ was 5-fold diluted in a 15 mM Tris-HCl buffor (pH = 8.2 and pH = 6) containing 0.025% *N*,*N*-dimethyldodecylamine-*N*-oxide (LDAO) and 1 mM EDTA. During the transient absorption experiment, the sample (~2.5 mL) was placed in a spinning quartz wheel of 10 cm in diameter, rotating at about 10 Hz in order to ensure full relaxation of the sample between laser flashes. The optical path of the laser beam in the sample was about 1.5 mm.

The transient absorption spectrometer, containing a 1 kHz femtosecond laser system (Ti:sapphire, Spectra Physics) and a grating polychromator (Spectra Pro 150, Acton Research Corp.) with a thermoelectrically cooled CCD camera (Back Illumin., Princeton Instruments) was described in detail in ref 15. Laser pulses of ~2 μJ energy, ~100 fs duration (full width at half-maximum, fwhm), and 15 nm spectral bandwidth centered at 800 nm were used to excite the sample with 1 kHz repetition rate. The pulses of white light generated in a calcium fluoride plate were used to probe absorption changes induced by the excitation pulses, in the spectral window from 330 to 700 nm. The transient absorption spectra were collected for pump−probe delay times up to 1 ns. The temporal step between 57 consecutive transient spectra was gradually increased from 100 fs for the shortest delays to 100 ps for the longest delays. The data were subjected to global analysis[16,17] by using the ASUFIT program (available at www.public.asu.edu/~laserweb/asufit/asufit.html).

Results

Figure 1 shows the decay associated spectra (DAS) of *Rb. sphaeroides* RCs with both free electron transfer (open RCs; panel A) and with blocked electron transfer from H_A^- to Q_A (closed RCs) either by removing Q_A (Figure 1B) or by reducing it (Figure 1C,D). In all four cases, we limited the number of exponential components to three plus a constant (nondecaying component, ND). Addition of another lifetime component, predicted in the model of two-step or heterogenic charge separation, resulted in the fit artifacts in some spectral subranges. The interpretation of the two fastest components was the same for all four sets of data: the subpicosecond component was assigned to the excitation energy transfer from B* to P,[18−22] and the 5.2−6.8 ps component was assigned to the primary

charge separation forming $P^+H_A^-$.[1,23−27] The 230 ps component associated with electron transfer from H_A^- to Q_A in open RCs was replaced in RCs with reduced quinone Q_A by the ∼700 ps component assigned to the fast phase of the $P^+H_A^-$ charge recombination. In RCs without Q_A, the respective component had very low amplitude. The nondecaying component was assigned to the $\Delta OD(P^+Q_A^- - PQ_A)$ signal in open RCs (Figure 1A),[28] and to the slow phase of the $P^+H_A^-$ charge recombination in closed RCs (Figure 1B−D). The results presented in Figure 1 were obtained for RCs dissolved in the buffer of pH = 8.2, but very similar spectra and lifetimes associated with these spectra were obtained at pH = 6 and can be found in the Supporting Information.

Comparison of the Primary Charge Separation in Open and Closed RCs. Signal to noise ratio of our experiment was insufficient to resolve more than one lifetime associated with the primary charge separation in whole investigated spectral range. Thus, the lifetimes of the few picosecond components presented in this paper should be regarded as average values contributed by the ∼3−4 and ∼10 ps primary charge separation phases known from the literature.[29,30]

The spectrum of charge separation is of similar shape for open and closed RCs (Figure 1A−D). The lifetime associated with this spectrum increases by ∼30% from 5.2 ps in open RCs to 6.8 ps in closed RCs (Figure 1A,C). The same ∼30% increase in the primary charge separation time after chemical reduction of Q_A by sodium dithionite was reported before.[23] Also, similar 6.1 ps lifetime of charge separation in Q_A-reduced RCs from *Rb. sphaeroides* was measured from decay of stimulated emission of P* between 870 and 1000 nm.[31] Addition of 10 mM *o*-phenanthroline to Q_A-reduced RCs slightly accelarates the primary charge separation to ∼6.4 ps. The effect of *o*-phenanthroline is not very big but reproducible as checked in a few independent experiments (also at pH = 6, see Supporting Information). We propose that the deceleration of the primary charge separation in Q_A-reduced RCs is caused by the negative charge on Q_A which is expected to influence the energetics of this reaction. This explanation is in line with the effect of *o*-phenanthroline which is known to mediate the protonation of titratable groups near Q_A,[10,11] thus partly screening the negative charges.

In RCs without Q_A, the charge separation time is 6.2 ps and is insignificantly changed after addition of *o*-phenanthroline. The value of 6.2 ps is greater than 5.2 ps characteristic of open RCs but this difference may be related to small structural changes caused by the removal of quinone Q_A.

230 ps DAS and Nondecaying Spectrum in Open Reaction Centers. Within 230 ps electron is transferred from H_A^- to Q_A. Therefore, absorption changes visible in the 230 ps DAS (Figure 1A) are a sum of the absorption changes caused by reoxidation of H_A^- and by reduction of Q_A. Similarly, the nondecaying spectrum is a sum of absorption changes caused by oxidation of P, $\Delta OD(P^+-P)$, and reduction of Q_A, $\Delta OD(Q_A^- - Q_A)$. It should be noted that the contribution of absorption changes originating from reduction of Q_A in both spectra is much smaller than those related to oxidation of P and H_A^- and limited to the blue spectral range.[32] Since the contributions of $\Delta OD(Q_A^- - Q_A)$ to the 230 ps DAS and to nondecaying spectra are identical but of opposite signs (the 230 ps DAS and ND component depict the kinetics of appearance and infinitesimally slow decay of Q_A^-, respectively), the sum of the two latter spectra represents absorption difference spectrum of the states $P^+H_A^-$ and PH_A, $\Delta OD(P^+H_A^- - PH_A)$, well-known from the literature.

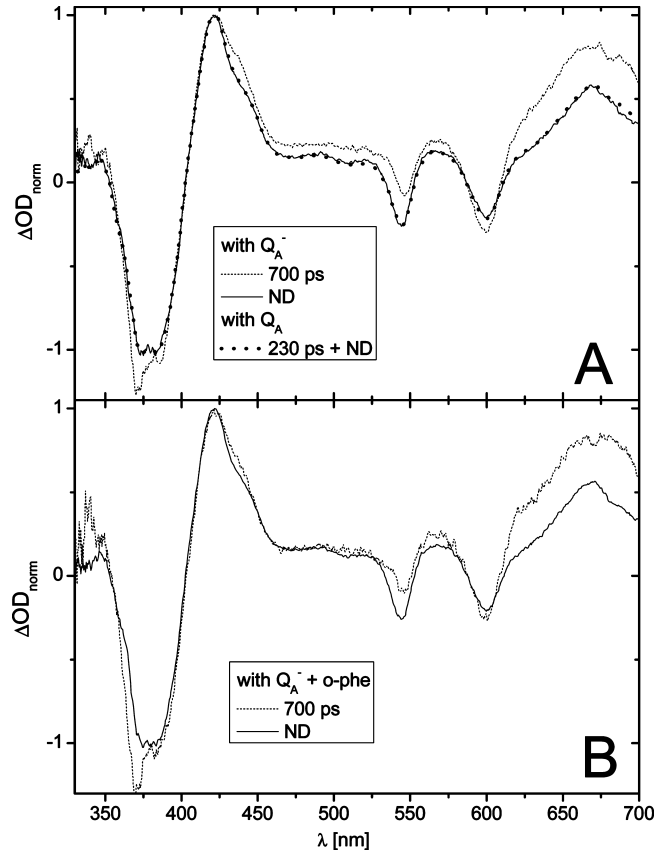

Figure 2. Comparison of the shapes of the subnanosecond and nondecaying charge recombination spectra from Figure 1 in Q_A-reduced RCs from *Rb. sphaeroides* before (A) and after (B) addition of 10 mM *o*-phenanthroline. The spectra were normalized to the same amplitude at the maximum of the ∼422 nm band. In panel A, the sum of the 230 ps spectrum and $\Delta OD(P^+Q_A^- - PQ_A)$ nondecaying spectrum obtained for open RCs (Figure 1A) is also shown after similar normalization at 422 nm.

Subnanosecond and Nondecaying Charge Recombination Components in Closed Reaction Centers. The shape of the nondecaying spectrum of RCs with Q_A^- (Figure 1C) is identical to that of the sum of the 230 ps DAS and the nondecaying spectrum of open RCs (Figures 1A and 2A). Since the latter sum has been assigned to the difference of absorption spectra of the states $P^+H_A^-$ and PH_A (see above), the identity of the shapes mentioned above allows the assignment of the nondecaying component in Q_A-reduced RCs to $\Delta OD(P^+H_A^- - PH_A)$. Since $P^+H_A^- \rightarrow PH_A$ charge recombination in closed RCs occurs in the nanosecond time range,[2−7] we assign the component nondecaying on 1 ns time scale to charge recombination. On the other hand, the shape of the 700 ps spectrum is similar to that of the nondecaying spectrum in Q_A-reduced RCs (Figure 2A), indicating that the subnanosecond component is due to the fast phase of the $P^+H_A^- \rightarrow PH_A$ charge recombination. This phase is visualized in Figure 3, in which the kinetic traces at 369, 668, and 420 nm are presented. The traces at the two former wavelengths represent relatively pure decay of the $\Delta OD(H_A^- - H_A)$ signal whereas the trace at 420 contains additionally contribution from the decay of the $\Delta OD(P^+-P)$ signal. The relationships between these two contributions at particular wavelengths are assessed from the amplitudes of the 230 ps DAS (representing mostly decay of the $\Delta OD(H_A^- - H_A)$ signal) and nondecaying component (representing mostly decay of the $\Delta OD(P^+-P)$ signal) in open RCs (Figure 1A).

The shapes of the subnanosecond and slow (ND) charge recombination spectra deviate somewhat from each other (Figure

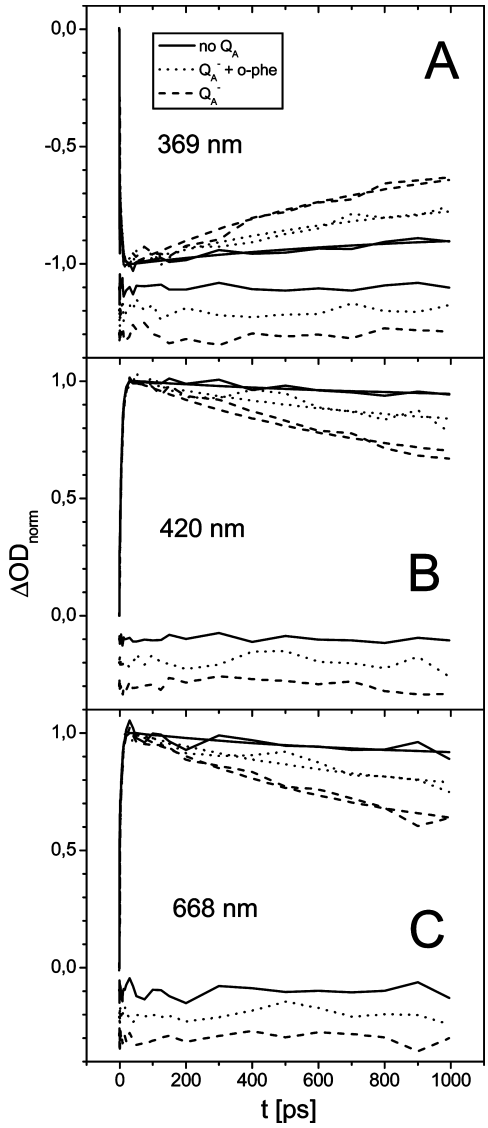

Figure 3. Kinetic traces of absorbance changes recorded at three different probe wavelengths at 800 nm excitation for three samples with closed RCs. The fits were extracted from the global analysis presented in Figure 1.

2A). This suggests that the two phases of the $P^+H_A^- \rightarrow PH_A$ charge recombination are related to RCs differing in their conformational states. Moreover, it is the fast phase that deviates from the shape of the "230 ps + ND" open RCs spectrum (Figure 2A), suggesting that the conformational state related to this phase and not to the slow one is different from the state characteristic of open RCs. The most pronounced spectral differences between the two charge recombination phases are different relative amplitudes of the ~544 and ~600 nm bands (the amplitude ratio of the 600/544 nm bands is about twice greater in the 700 ps spectrum) and a larger amplitude of the strong anionic band around 670 nm in the 700 ps spectrum (Figure 2A).

The integrated area of the 700 ps spectrum is somewhat smaller than that of the nondecaying component in Q_A-reduced RCs (47% vs 53%; Figure 1C and Table 2). Addition of 10 mM *o*-phenanthroline causes a significant decrease in the contribution of the fast charge recombination phase (to ~27%; compare panels C and D in Figure 1). On the other hand, the addition of this herbicide does not affect the shapes of the fast and slow charge recombination spectra (Figure 2).

The subnanosecond spectrum of the Q_A-removed RCs is characterized by significantly smaller amplitude, shorter lifetime and the shape somewhat different than those of Q_A-reduced RCs (Figure 1B). Careful comparison of the shapes of the few hundred picosecond spectra in panels A, B, and C leads to the conclusion that the 430 ps DAS (Figure 1B) has the shape intermediate between that of the 230 ps DAS (Figure 1A) and that of the 700 ps DAS (Figure 1C). Also the value of 430 ps is between 230 and 700 ps. Both these observations indicate that the small 430 ns component is due to a mixture of two processes. One of them is electron tranfser from H_A^- to Q_A in a very minor fraction of the "Q_A-removed RCs" still containing Q_A. This fraction is estimated to be below 10%. Another process possibly contributing to this DAS is the fast, subnanosecond, charge recombination occurring in a very minor fraction of RCs, estimated to be also below 10%.

The shape of the nondecaying component for the Q_A-removed RCs is very similar to the respective component of the Q_A-reduced RCs (Figure 1B,C). This similarity demonstrates the same process of slow charge recombination, occurring on the time scale longer than that of our experiment. Minor differences between these two spectra are due to a small admixture of the ($P^+Q_A^- - PQ_A$) signal in "Q_A-removed" RCs resulting from a minor fraction of RCs still containing Q_A. Addition of 10 mM *o*-phenanthroline to the sample with Q_A-removed RCs has no significant effect on the lifetimes, shapes, and relative amplitudes of the DAS and of the nondecaying components resulting from the global analysis (data not shown).

In general, for all closed RCs under study, the spectral shapes of both phases of the charge recombination resemble the mirror reflections of the charge separation spectra (Figure 1B−D). This symmetry is expected since the charge separation and charge recombination are two opposite processes involving, respectively, the formation and the decay of the same species, P^+ and H_A^- (eq 1). The symmetry is somewhat broken mostly by the contribution of absorption changes from P* (in the Soret and Q_x regions) in the charge separation DAS.

Discussion

The primary charge recombination in purple bacterial RCs was, until recently, regarded as an essentially monophasic process occurring from the relaxed form of the primary radical pair $P^+H_A^-$ with 10−30 ns lifetime.[2−7] The relaxation of the $P^+H_A^-$ state was inferred from the multiphasic fluorescence decay occurring on the subnanosecond to nanosecond time scales.[14,33,34] Recently, we have reported results of the transient absorption measurements performed on the nano- to microsecond time scales with the 1 ns temporal resolution, demonstrating the multiexponential decay of the $\Delta OD(P^+ - P)$ signal at 970 and 1300 nm modeled with the <1, 3−4, and 9−12 ns time constants.[9] These data were interpreted in terms of the coexistence of three conformational states of RCs characterized by different charge recombination dynamics (an alternative interpretation of this multiphasic kinetics related to relaxation of the free energy level of the state $P^+H_A^-$, also was discussed in ref 9). The equilibrium between the three conformational states was proposed to be controlled by the electrical charges in the site Q_A: both the negative charge on Q_A^- and the charges of the ionizable amino acid side chains in the Q_A pocket. In the following we extend this model to explain the results of ultrafast transient absorption measurements performed in the 1 ns temporal window.

Charge Recombination. The subnanosecond charge recombination was clearly resolved in these studies for Q_A-reduced

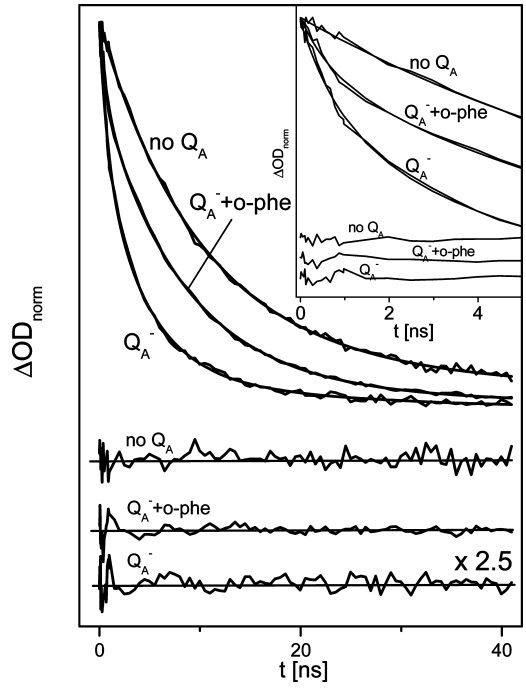

Figure 4. Kinetic traces constructed from the data collected at 420 nm in 1 ns temporal range (from Figure 3B) and at 970 nm from 1 to 40 ns for three samples with closed RCs. The fits were performed in the time range from 30 ps (at this time delay, the charge separation is completed and the only process observed is charge recombination) to 80 ns and are shown together with residuals. The experimental data were fitted with a sum of two (RCs without Q_A) or three (two remaining samples) exponential decays plus a constant: $\sum A_i \exp(-t/\tau_i)$ + const. Fit parameters: (no Q_A) 9 ± 1 ns (65%), 18 ± 6 ns (26%), const (9%); (Q_A^-) 0.83 ± 0.08 ns (30%), 4.3 ± 0.4 ns (56%), 20 ± 5 ns (10%), const (4%); (Q_A^- + *o*-phenanthroline) 0.63 ± 0.05 ns (16%), 8.0 ± 0.4 ns (72%), 25 ± 14 ns (7%), const (5%). Inset: temporal zoom of the data, fits, and residuals presented in the main panel.

RCs and was fitted with a time constant of ~700 ps (Figure 1C,D). Due to the temporal window of our setup limited to 1 ns, the exact lifetime and amplitude of this component remained still somewhat uncertain. In order to extend the temporal window, we combined the kinetic traces presented in Figure 3 with those measured previously in 80 ns temporal window at 970 nm.[9] Since both in the visible and at 970 nm the same process of $P^+H_A^- \rightarrow PH_A$ charge recombination is observed, combining the kinetic traces obtained at different wavelengths is justified. The kinetic traces combined from the data measured at 420 nm in 1 ns temporal window and at 970 nm on longer time scale are presented in Figure 4 together with fit curves, fit parameters, and residuals. Similar combination of the slow kinetics at 970 nm and fast kinetics at 369, 454, and 668 nm resulted in similar fit parameters which are summarized in Table 1. The fit parameters in Table 1 confirm contribution of the subnanosecond component of ~(700 ± 200) ps. The amplitudes of this phase, ~26% for Q_A-reduced RCs and ~13% for Q_A-reduced RCs with *o*-phenanthroilne, are somewhat lower than those resulting from the global fitting (Figure 1C,D, Table 2). These differences are related to the fact that, in the global analysis procedure, the slow charge recombination was fixed as a nondecaying component and therefore the contribution of the subnanosecond component was somewhat overestimated. On the other hand, leaving the slowest decay component in the global analysis as a free parameter or fixing it on a level of a few nanoseconds gave unreliable solutions due to the temporal range of the experimental data limited to 1 ns.

TABLE 1: Results of Multiexponential Fitting of the Combined Absorption Changes Measured at 369, 420, 454, and 668 nm in 1 ns Temporal Window and at 970 nm in 80 ns Temporal Window (Data Taken from Ref 9)[a]

sample	lifetime (ns)	rel amplitude (%)
Q_A^-	0.5−0.9	23−29
	3.7−4.3	56−64
	12−16	9−13
	const	3−4
Q_A^- + *o*-phenanthroline	0.4−0.7	10−16
	7.6−8.2	68−81
	19−30	6−11
	const	~5
without Q_A	0.2−0.3	0−4
	9−12	65−90
	17−24	0−26
	const	5−9

[a] The ranges of the values reflect somewhat different fit parameters resulting from combining the data at 970 nm with those obtained at four different wavelengths in the visible.

TABLE 2: Contributions of the Subnanosecond $P^+H_A^- \rightarrow PH_A$ Charge Recombination in Closed RCs with and without Addition of 10 mM *o*-Phenanthroline[a]

sample		Q_A^-	Q_A^- + *o*-phenanthroline	without Q_A
contribution of subnanosecond charge recombination (%)	Gibasiewicz and Pajzderska, 2008	77	47	40
	1 ns range	47	27	<10
	1 ns + 80 ns range	~26	~13	<5

[a] The contributions in 1 ns range were calculated from the formula $A_{700}/(A_{700} + A_{ND})$, where A_{700} is the integrated area of the ~700 ps charge recombination spectrum, and A_{ND} is the integrated area of the nondecaying charge recombination spectrum (Figure 1B−D). The contributions in the combined "1 ns + 80 ns range" are taken from Table 1.

The relative contributions of the subnanosecond charge recombination found from the fits performed in 1 ns range and combined 1 ns plus 80 ns range should also be compared to those published previously[9] (Table 2). In these previous studies, the subnanoscond component was found from the deconvolution procedure applied in the analysis of the data collected with the 1 ns temporal resolution. Apparently, contributions of this component were overestimated in ref 9 (Table 2) but it is not much surprising since the temporal resolution in the previous study was insufficient to determine accurately the amplitude of such a fast phase. A common important feature of all the data sets in Table 2 is that the contribution of the subnanosecond charge recombination is modulated by the electrical charges at the site Q_A (Figure 1B−D): it is the highest for RCs with Q_A^- (Figure 1C), intermediate for RCs with Q_A^- after addition of *o*-phenanthroline (Figure 1D), and the lowest for RCs without Q_A (Figure 1B).

The remaining two, 3−4 and 12 ns, phases of the charge recombination, reported in ref 9 for both Q_A-reduced and Q_A-removed RCs, naturally could not be resolved in the present studies performed in 1 ns temporal window. Instead, they are lumped together and seen as one nondecaying component (Figure 1B−D). In the combined fits (Figure 4, Table 1), the lifetimes originating from the multiexponential analysis and associated with slow charge recombination are somewhat different from those published previously[9] due to constraints superimposed on the fits by the experimental results measured within first nanosecond. RCs with Q_A^-, Q_A^- plus *o*-phenanthroline, and without Q_A are dominated by ~4, ~8, and ~11

ns decays, respectively (Table 1), whereas the slowest components are of minor amplitudes.

The two charge recombination phases resolved in 1 ns temporal window (Figure 1C,D), in line with the previous model,[9] are assigned to separate subpopulations of RCs characterized by conformational states differing from each other also spectrally (Figure 2). The size of the "fast charge recombination" subpopulation is correlated with the load of the negative charge at the site Q_A. Both of them are the highest when Q_A is reduced, lowered after addition of *o*-phenanthroline, and very low when there is no Q_A. However, even for the Q_A-reduced RCs, a large fraction of RCs show slow charge recombination kinetics similar to that one observed in the Q_A-removed RCs (Figure 1C,D). All these observations can be consistently explained by the simple model relating the two conformational states of RCs with a protonation state of a single titratable group in the Q_A site. If this group is protonated, and thus the negative charge on Q_A is neutralized, the slow charge recombination occurs. Otherwise, the fast (subnanosecond) charge recombination takes place. Thus, the lack of the negative charge on Q_A in the Q_A-removed RCs explains the domination of the slow charge recombination in this case. Also, the lack of the negative charge on Q_A in open RCs explains the identical shapes of the sum of $\Delta OD(H_A^- - H_A)$ and $\Delta OD(P^+ - P)$ spectra and the slow charge recombination spectrum (Figure 2A). The slightly different shape of the fast charge recombination spectrum (Figure 2A,B), in addition to the short lifetime, reveals the effect of the noncompensated negative charge. The coexistence of both phases in the Q_A-reduced RCs indicates that p*K* value of the hypothetical titratable group is close to the local pH at the Q_A site and, thus, similar fractions of RCs remain in the protonated and unprotonated states. In line with this reasoning, relative contributions of the fast and slow charge recombination (Table 2, 1 ns range) can be used to estimate the p*K* value of the titratable group from the Henderson−Hasselbach equation

$$pK = pH - \log(A/B) \qquad (2)$$

where *A* and *B* are the concentrations of the unprotonated and protonated forms of the titratable group. By substituting *A* and *B* with the relative amplitudes of the fast and slow phase, respectively, and assuming pH at the site Q_A the same as that of the buffer used (8.2), one can obtain p*K* = ∼8.3 for the Q_A-reduced RCs and ∼8.7 after addition of *o*-phenanthroline. Using contributions of fast and slow recombination from an alternative combined fit (Table 1, 1 ns + 80 ns range) makes only a small difference in the respective p*K* shift from 8.5 to 8.9. A positive shift of p*K* of similar value (∼0.4 p*K* unit), from ∼9.7 to ∼10.1, after addition of *o*-phenanthroline was previously reported for Q_A/Q_A^- in *Rhodobacter sphaeroides*.[10] On the other hand, a positive shift of p*K*, from 7.5 to 8.7 and from 8.5 to 9.0, of the hypothetical titratable amino acid residue situated close to Q_A in, respectively, two conformational states of RCs from *Rhodopseudomonas viridis* was reported after addition of *o*-phenanthroline.[11,35] These reports suggest that the titratable group responsible for two conformational states of RCs reported by us may be either Q_A^- itself or a side chain of a nearby amino acid residue.

In order to verify the hypothesis that the protonation state of the titratable site near Q_A modulates the relative contributions of the fast and slow phases of charge recombination we performed a series of experiments at pH = 6 (see Supporting Information). At low pH we expected full protonation of the titratable group discussed above. Unexpectedly, the contributions of both phases of charge recombination was almost the same as at pH = 8.2. A possible explanation of this observation is that pH outside RC has no significant effect on the local pH near Q_A.

On the basis of our data we cannot completely rule out the possibility that the biphasic charge recombination observed in 1 ns temporal window (and three-phasic charge recombination observed on longer time scale) originates from the pH-independent static heterogeneity of RC conformation or dynamic relaxation of the state $P^+H_A^-$.[7,14,33,34] However, the observed effect of *o*-phenanthroline suggests static heterogeneity of RCs related to different protonation states of the titratable residues.[11,36] More detailed discussion on dynamic relaxation vs static heterogeneity model was presented in ref 9.

Primary Charge Separation. The coexistence of two conformational states of RCs in preparations with Q_A reduced, clearly detected on the charge recombination time scale (Figure 1C,D), is more difficult to observe experimentally on the time scale of the primary charge separation. A possible reason for this difficulty may be that the temporal separation of the charge separation lifetimes related to the two conformational forms of RCs is much smaller than that of the subnanosecond and nanosecond charge recombination phases. Moreover, the charge separation is in fact multiexponential even for homogeneous conformational state of RCs[26,27,29,30] that makes the trials to resolve components belonging to two different conformational states practically hopeless. Nevertheless, the increase in the average lifetime from 5.2 to 6.8 after reducing the RCs may be interpreted as the effect of an appearance of two conformational states, both with similar slowed charge separation or with two different charge separation lifetimes. We favor the latter possibility for the following reason. As we noticed above, the "slow charge recombination" conformation assigned to the state with neutralized charge on Q_A has got identical long-time spectral properties as the conformation characteristic of the open RCs (Figure 2A). Thus, it is reasonable to assume that the charge separation in this conformation, even after prereduction of Q_A, remains unchanged and is still close to 5.2 ps. Then, the value of 6.8 ps observed in Q_A-reduced RCs would be an average of the ∼5.2 ps and a few picoseconds longer another charge separation lifetime characteristic of the "fast charge recombination" conformation, weighted with relative contributions of the two subpopulations of RCs. Consistent with this reasoning, addition of *o*-phenanthroline, which decreases the contribution of the "fast charge recombination" subpopulation, should result in the decrease of the experimentally measured averaged primary charge separation lifetime, and this is indeed observed (Figure 1, C and D).

$P^+B_A^- \leftrightarrow P^+H_A^-$ Equilibrium Model. The three-exponential decay of $P^+H_A^-$ measured on the nanosecond time scale has been recently proposed to occur via the thermally accessible $P^+B_A^-$ state.[9] Earlier, a similar thermally activated mechanism was proposed both for $P^+H_A^{-2}$ and for $P^+Q_A^-$ and $P^+Q_B^-$ charge recombination.[14,35,37−41] Hereby, we adopt the idea of $P^+B_A^- \leftrightarrow P^+H_A^-$ thermal equilibrium to model the charge recombination reaction studied in the 1 ns temporal window. This model may be applied independently of the interpretation of the different phases of charge recombination (static distribution of conformational states or dynamic relaxation of the state $P^+H_A^-$) as it was discussed in ref 9.

In order to roughly estimate an equilibrium concentration of the states $P^+H_A^-$ and $P^+B_A^-$ on the 700 ps charge recombination time scale we have made a few following assumptions. First, we assumed that the steady-state absorption band at 544 nm is

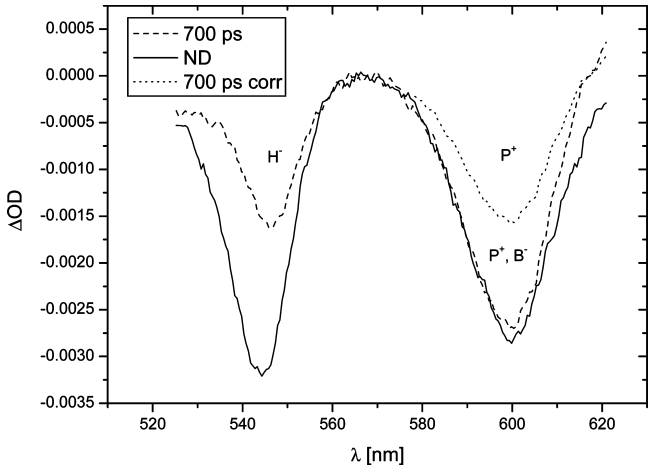

Figure 5. Comparison of the relative amplitudes and shapes of the 544 and 600 nm bands of the two charge recombination spectra in Q_A-reduced RCs: subnanosecond (700 ps) and nondecaying (ND; see Figure 1C). Both spectra were vertically shifted to zero at ~570 nm to facilitate integration of the areas over the bands. Additionally, the 600 nm band of the subnanosecond spectrum was divided onto two compartments: the upper one contributed by P^+ (from $P^+H_A^-$) and the lower one contributed by P^+ and B_A^- (from $P^+B_A^-$). See text for further details.

contributed exclusively by BPhe H, whereas the band at ~600 nm is contributed by BChls forming P and B. Consequently, the negative bands at 544 and 600 nm of the ~700 ps and ND charge recombination spectra (Figure 1C,D) may serve to estimate the equilibrium populations of the states $P^+H_A^-$ and $P^+B_A^-$ in the respective time scales. The decay of H_A^- (due to charge recombination) should be manifested by the decay of photobleaching of the 544 nm band, whereas the decay of P^+ and B_A^- should result in decay of photobleaching of the 600 nm band. In consequence, the decay of $P^+B_A^-$ should show a single negative band at ~600 nm, whereas the decay of $P^+H_A^-$ should show two negative bands: at 544 and at ~600 nm. We propose that the different relative amplitudes of these two negative bands for the ~700 ps and nondecaying spectra (Figures 1C,D and 2A,B) are a result of different contributions of the state $P^+B_A^-$ in these two spectra. Our second assumption, necessary to perform simple calculations, is that the amount of the RCs in the state $P^+B_A^-$, being in equilibrium with the state $P^+H_A^-$, may be neglected on the long time scale corresponding to the nondecaying component but is significant on 700 ps time scale. As shown below this assumption is justified: ~30% of Q_A-reduced RCs is in the state $P^+B_A^-$ on 700 ps time scale, and only ~6% on longer time scale. This implicates that the negative band at ~600 nm in the nondecaying spectra is contributed exclusively by P^+ from $P^+H_A^-$ state (Figure 1C,D). On the other hand, the band at ~600 nm in the ~700 ps DAS (greater than that in the nondecaying spectrum relative to the 544 nm band) contains an additional contribution from B_A^- and P^+ originating from the state $P^+B_A^-$.

Figure 5 presents our approach for estimating relative populations of Q_A-reduced RCs with $P^+B_A^-$ and $P^+H_A^-$ undergoing ~700 ps charge recombination. In agreement with the above assumptions, only an upper part of the ~600 nm band (above the dotted line) of the ~700 ps spectrum represents the contribution from P^+ originating from the subpopulation of RCs being in the $P^+H_A^-$ state. One can note that the ratio of peak amplitudes of the bands at 544 (dashed) and 600 nm (dotted) of the 700 ps spectrum is the same as the respective ratio in the nondecaying spectrum (solid). The remaining part of the 600 nm band (below the dotted line) represents the contribution from B_A^- and P^+ originating from the other subpopulation of RCs being in the $P^+B_A^-$ state. Half of this remaining part was attributed to $\Delta OD(P^+-P)$ and half to $\Delta OD(B_A^- - B_A)$ (assuming the same differential extinction coefficients for P^+-P and for $B_A^- - B_A$). From the integrated areas related to P^+ from $P^+H_A^-$ and from $P^+B_A^-$ within the 600 nm band we calculated relative populations of the RCs with $P^+H_A^-$ and $P^+B_A^-$. Next, using the Boltzman distribution, we estimated free energy difference between these states in the fraction of RCs undergoing the ~700 ps charge recombination (Table 3). The same procedure was applied for Q_A-reduced RCs with addition of *o*-phenanthroline (Table 3). It turned out that despite significant drop in the population of RCs with $P^+H_A^-$ recombining in 700 ps in response to the addition of *o*-phenanthroline (Figure 1C,D and Table 2) the free energy gap between $P^+H_A^-$ and $P^+B_A^-$ was not significantly altered by this herbicide. Interestingly, the values of this gap, 21−27 meV, are small, comparable with those of the initial gap between these states of 0−75 meV[42−48] (on the charge separation time scale) suggesting that both $P^+H_A^-$ and $P^+B_A^-$ states undergo similar energetic relaxation within first nanosecond after excitation.

TABLE 3: Contributions of the States $P^+H_A^-$ and $P^+B_A^-$ to the 600 nm Band of the 700 ps Charge Recombination Spectra and Free Energy Difference between These States (See Figure 5 and Text for Details)

	Q_A^-	Q_A^- + *o*-phenanthroline
$A_{600}(P^+H_A^-)/A_{600}(P^+B_A^-)$ (%)	70/30	74/26
ΔG (meV)	21	27

Assumptions underlying our calculations described above should be confronted with earlier experimental observations. It has been shown that direct excitation of the B band at 800 nm leads, in a small fraction of RCs, to formation of the primary radical pairs, possibly including $B_A^+H_A^-$, without intermediate formation of P*.[49,50] However, even if such a radical pair is formed it is very unlikely that it persists on a time scale of charge recombination and influences our calculations. A possible small bleaching at 600 nm caused by reduction of H_A has been neglected resulting in a possible underestimation of the concentration of the $P^+B_A^-$ state being in equilibrium with the $P^+H_A^-$ state.

The deep internal electrostatic modulation of the $P^+H_A^- \rightarrow PH_A$ charge recombination kinetics together with the modulation of the $P^+H_A^- \leftrightarrow P^+B_A^-$ equilibrium shown above indicate that the charge recombination occurs predominantly via the thermally activated state $P^+B_A^-$, at least at room temperature. Having the 21−27 meV value of $\Delta G(P^+B_A^- - P^+H_A^-)$ for the RCs showing the ~700 ps charge recombination, and knowing the lifetimes of the two longer charge recombination phases from the combined fits (Figure 4), we may estimate the parameters of the model assuming the coexistence of RCs in three conformational states characterized by different free energy gaps between $P^+H_A^-$ and $P^+B_A^-$.[9] Figure 6 summarizes our calculations. The intrinsic charge recombination lifetime from the state $P^+B_A^-$ to the ground state, $\tau_i \approx 200$ ps, was estimated from the formula

$$\tau_i = \tau[1 + \exp(\Delta G/k_B T)]^{-1} \quad (3)$$

where $\Delta G = 21-27$ meV, $\tau = 600-800$ ps, k_B is the Boltzmann constant, and T is absolute temperature. The value of $\tau_i \approx 200$ ps is more precisely determined than previously (15−400 ps).[9]

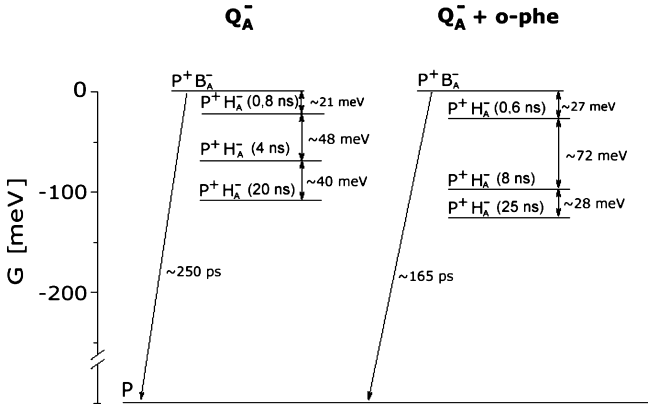

Figure 6. Free energy gaps between $P^+B_A^-$ and $P^+H_A^-$ calculated on the charge recombination time scales for Q_A-reduced RCs (without and with 10 mM *o*-phenanthroline). The lifetimes of the $P^+H_A^- \rightarrow PH_A$ charge recombination were taken from Figure 4.

This ~200 ps value is similar to that of the $P^+B_B^-$ charge recombination reported for the BChl (B_B) → BPhe (B_B) mutant[51] and smaller than the 675 ps charge recombination of $P^+B_A^-$ in the Phe to Asp(L121) mutant of *Rb. sphaeroides*.[52] The same eq 3 was then used to calculate the free energy gaps, ΔG, between $P^+B_A^-$ and lower lying $P^+H_A^-$ states. Equilibrium concentrations of the RCs in the state $P^+B_A^-$ estimated from these gaps for the fastest, intermediate, and slowest charge recombination conformations are respectively 30%, 6%, and 1% for Q_A-reduced RCs, and 26%, 2%, and 0.7% for Q_A-reduced RCs with of *o*-phenanthroline. Assuming that in open RCs charge recombination occurs within ~10 ns, similarly as in RCs with removed Q_A, whereas electron from H_A^- to Q_A is transferred within ~200 ps, it is easy to calculate that the efficiency of the forward reaction is ~98%.

The two or three subpopulations or conformational states of RCs (resolved in 1 ns and 1 ns + 80 ns temporal windows, respectively) differing in the rate of charge recombination and free energy levels of $P^+H_A^-$ were impossible to resolve kinetically and spectrally (as discussed above), and also energetically on the charge separation time scale. The overall effect of the negative charge on Q_A^- on the charge recombination time scale is an upshift of the average free energy of the state $P^+H_A^-$ (weighted with the populations of particular $P^+H_A^-$ substates) relative to that of the $P^+B_A^-$ state. This upshift was observed before[9] and may be easily concluded from the comparison of the data for Q_A-removed and Q_A-reduced RCs (Table 1). On the other hand, the screening effect of *o*-phenanthroline decreases this upshift both by decreasing the population of quickly recombining conformation (in ~700 ps) and by slowing recombination lifetime associated with the intermediate conformation from ~4 to ~8 ns (Table 1, Figure 6). Similar upshift of the averaged $P^+H_A^-$ level in Q_A-reduced RCs is expected on the charge separation time scale and is consistent with the observed increase of the charge separation lifetime in Q_A-reduced RCs.

The free energy upshift of the averaged state $P^+H_A^-$ on the time scales of both charge separation and charge recombination gives opposite effects on the rates of these two reactions: deceleration of the primary charge separation and acceleration of the charge recombination. These opposite effects are expected since the upshift decreases the driving force, $\Delta G(P^*-P^+H_A^-)$, of the former reaction and at the same time shifts the free energy level of the $P^+H_A^-$ state closer toward the quickly recombining $P^+B_A^-$ state.

Abbreviations: B, B_A, accessory bacteriochlorophyll; BChl, bacteriochlorophyll; BPhe, bacteriopheophytin; DAS, decay-associated spectrum; H, H_A, primary electron acceptor; ND, nondecaying; P, primary electron donor; RC, reaction center.

Acknowledgment. The authors are very thankful to Neal Woodbury and Haiyu Wang for providing the samples, reading the manuscript, and valuable comments. K.G. acknowledges financial support from the Polish government (project entitled "Electrostatic control of electron transfer in purple bacteria reaction center") and the technical assistance of Margareta Gibasiewicz.

Supporting Information Available: Figure showing decay-associated spectra of RCs at pH = 6. This material is available free of charge via the Internet at http://pubs.acs.org.

References and Notes

(1) Woodbury, N. W. T.; Allen, J. P. Electron transfer in purple nonsulfur bacteria. In *Anoxygenic Photosynthetic Bacteria*; Blankenship, R. E., Madigan, M. T., Bauer, C. E., Eds.; Kluwer Academic Publishers: Dordrecht, The Netherlands, 1995; p 527.

(2) Shuvalov, V. A.; Parson, W. W. *Proc. Natl. Acad. Sci. U.S.A.* **1981**, *78*, 957.

(3) Schenck, C. C.; Blankenship, R. E.; Parson, W. W. *Biochim. Biophys. Acta* **1982**, *680*, 44.

(4) Chidsey, C. E. D.; Kirmaier, C.; Holten, D.; Boxer, S. G. *Biochim. Biophys. Acta* **1984**, *766*, 424.

(5) Budil, D. E.; Kolaczkowski, S. V.; Norris, J. R. The temperature dependence of electron back-transfer from the primary radical pair of bacterial photosynthesis. In *Progress in Photosynthesis Research*; Biggens, J., Ed.; Martinus Nijhoff Publishers: Dordrecht, The Netherlands, 1987; Vol. 1, p 25.

(6) Ogrodnik, A.; Volk, M.; Letterer, R.; Feick, R.; Michel-Beyerle, M. E. *Biochim. Biophys. Acta* **1988**, *936*, 361.

(7) Tang, C. K.; Williams, J. C.; Taguchi, A. K. W.; Allen, J. P.; Woodbury, N. W. *Biochemistry* **1999**, *38*, 8794.

(8) Volk, M.; Ogrodnik, A.; Michel-Beyerle, M. E. The recombination dynamics of the radical pair P^+H^- in external magnetic and electric fields. In *Anoxygenic Photosynthetic Bacteria*; Blankenship, R. E., Madigan, M. T., Bauer, C. E., Eds.; Kluwer Academic Publishers: Dordrecht, The Netherlands, 1995; p 595.

(9) Gibasiewicz, K.; Pajzderska, M. *J. Phys. Chem. B* **2008**, *112*, 1858.

(10) Prince, R. C.; Dutton, P. L. Protonation and the reducing potential of the primary electron acceptor. In *The photosynthetic bacteria*; Clayton, R. K., Sistrom, W. R., Eds.; Plenum Press: New York, 1978; p 439.

(11) Baciou, L.; Rivas, E.; Sebban, P. *Biochemistry* **1990**, *29*, 2966.

(12) Goldsmith, J. O.; Boxer, S. G. *Biochim. Biophys. Acta* **1996**, *1276*, 171.

(13) Okamura, M. Y.; Isaacson, R. A.; Feher, G. *Proc. Natl. Acad. Sci. U.S.A.* **1975**, *79*, 3491.

(14) Woodbury, N. W. T.; Parson, W. W.; Gunner, M. R.; Prince, R. C.; Dutton, P. L. *Biochim. Biophys. Acta* **1986**, *851*, 6.

(15) Maciejewski, A.; Naskrecki, R.; Lorenc, M.; Ziolek, M.; Karolczak, J.; Kubicki, J.; Matysiak, M.; Szymanski, M. *J. Mol. Struct.* **2000**, *555*, 1.

(16) Holzwarth, A. R. Data analysis of time-resolved measurements. In *Biophysical Techniques in Photosynthesis. Advances in Photosynthesis Research*; Amesz, J., Hoff, A. J., Eds.; Kluwer Academic Publishers: Dordrecht, The Netherlands, 1996; p 75.

(17) Van Stokkum, I. H. M.; Larsen, D. S.; van Grondelle, R. *Biochim. Biophys. Acta* **2004**, *1657*, 82.

(18) Jia, Y.; Jonas, D. M.; Joo, T.; Nagasawa, Y.; Lang, M. J.; Fleming, G. R. *J. Phys. Chem.* **1995**, *99*, 6263.

(19) Jonas, D. M.; Lang, M. J.; Nagasawa, Y.; Joo, T.; Fleming, G. R. *J. Phys. Chem.* **1996**, *100*, 12660.

(20) Stanley, R. J.; King, B.; Boxer, S. G. *J. Phys. Chem.* **1996**, *100*, 12052.

(21) King, B. A.; McAnaney, T.; deWinter, A.; Boxer, S. G. *J. Phys. Chem. B* **2000**, *104*, 8895.

(22) Jordanides, X. J.; Scholes, G. D.; Fleming, G. R. *J. Phys. Chem. B* **2001**, *105*, 1652.

(23) Woodbury, N. W.; Becker, M.; Middendorf, D.; Parson, W. W. *Biochemistry* **1985**, *24*, 7516.

(24) Martin, J.-L.; Breton, J.; Hoff, A. J.; Migus, A.; Antonetti, A. *Proc. Natl. Acad. Sci. U.S.A.* **1986**, *83*, 957.

(25) Breton, J.; Martin, J.-L.; Migus, A. *Proc. Natl. Acad. Sci. U.S.A.* **1986**, *83*, 5121.

(26) Holzapfel, W.; Finkele, U.; Kaiser, W.; Oesterhelt, D.; Scheer, H.; Stilz, H. U.; Zinth, W. *Chem. Phys. Lett.* **1989**, *160*, 1.
(27) Holzapfel, W.; Finkele, U.; Kaiser, W.; Oesterhelt, D.; Scheer, H.; Stilz, H. U.; Zinth, W. *Proc. Natl. Acad. Sci. U.S.A.* **1990**, *87*, 5168.
(28) Parson, W. W.; Clayton, R. K.; Cogdell, R. J. *Biochim. Biophys. Acta* **1975**, *387*, 265.
(29) Wang, H.; Lin, S.; Woodbury, N. W. *J. Phys. Chem. B* **2006**, *110*, 6956.
(30) Du, M.; Rosenthal, S. J.; Xie, X. J.; Dimagno, T. J.; Schmidt, M.; Hanson, D. K.; Schiffer, M.; Norris, J. R.; Fleming, G. R. *Proc. Natl. Acad. Sci. U.S.A.* **1992**, *89*, 8517.
(31) Wang, S.; Lin, S.; Lin, X.; Woodbury, N. W.; Allen, J. P. *Photosynth. Res.* **1994**, *42*, 203.
(32) Bensasson, R.; Land, E. J. *Bichim. Biophys. Acta* **1973**, *325*, 175.
(33) Woodbury, N. W. T.; Parson, W. W. *Biochim. Biophys. Acta* **1984**, *767*, 345.
(34) Woodbury, N. W. T.; Parson, W. W. *Biochim. Biophys. Acta* **1986**, *850*, 197.
(35) Sebban, P.; Wraight, C. A. *Biochim. Biophys. Acta* **1989**, *974*, 54.
(36) Fufezan, C.; Drepper, F.; Juhnke, H. D.; Lancaster, C. R. D.; Un, S.; Rutherford, A. W.; Krieger-Liszkay, A. *Biochemistry* **2005**, *44*, 5931.
(37) Kleinfeld, D.; Okamura, M. Y.; Feher, G. *Biophys. J.* **1985**, *48*, 849.
(38) Gopher, A.; Blatt, Y.; Schonfeld, M.; Okamura, M. Y.; Feher, G. *Biophys. J.* **1985**, *48*, 311.
(39) Gunner, M. R.; Robertson, D. E.; Dutton, P. L. *J. Phys. Chem.* **1986**, *90*, 3183.
(40) Shopes, R. J.; Wraight, C. A. *Biochim. Biophys. Acta* **1987**, *893*, 409.
(41) Sebban, P. *FEBS Lett.* **1988**, *233*, 331.
(42) Holzwarth, A. R.; Mûller, M. G. *Biochemistry* **1996**, *35*, 11820.
(43) Parson, W. W.; Chu, Z.; Warshel, A. *Biochim. Biophys. Acta* **1990**, *1017*, 251.
(44) Bixon, M.; Jortner, J.; Michel-Beyerle, M. E. In *The Photosynthetic Bacterial Reaction Center II*; Breton, J., Vermeglio, A., Eds.; Plenum: New York, 1992; p 291.
(45) Bixon, M.; Jortner, J.; Michel-Beyerle, M. E. *Chem. Phys.* **1995**, *197*, 389.
(46) Nagarajan, V.; Parson, W. W.; Davis, D.; Schenck, C. C. *Biochemistry* **1993**, *32*, 12324.
(47) Schmidt, S.; Arlt, T.; Hamm, P.; Huber, H.; Nagele, T.; Wachtveitl, J.; Meyer, M.; Scheer, H.; Zinth, W. *Chem. Phys. Lett.* **1994**, *223*, 116.
(48) Kirmaier, C.; Laporte, L.; Schenck, C. C.; Holten, D. *J. Phys. Chem.* **1995**, *99*, 8910.
(49) Lin, S.; Taguchi, A. K. W.; Woodbury, N. W. *J. Phys. Chem.* **1996**, *100*, 17067.
(50) Vos, M. H.; Breton, J.; Martin, J.-L. *J. Phys. Chem. B,* **1997**, *101*, 9820.
(51) Katilius, E.; Turanchik, T.; Lin, S.; Taguchi, A. K. W.; Woodbury, N. W. *J. Phys. Chem. B* **1999**, *103*, 7386.
(52) Heller, B. A.; Holten, D.; Kirmaier, C. *Biochemistry* **1996**, *35*, 15418.

JP811234Q